Asian Journal of Current Research in Clinical Cancer
ISSN: 3062-4444
2021, Volume 1, Issue 2, Page No: 41-55

Available online at: www.galaxypub.co/page/journals

Galaxy Publication

Galaxy Publication

Clinical Application of Quantitative Non-Invasive Ultrasound Techniques in Cancer Imaging

H. Al-Farsi[1*], K. Bader[1], S. Hassan[3]

[1]Department of Medical Oncology, College of Medicine, King Saud University, Riyadh, Saudi Arabia.

***E-mail** ✉ oncology.corresp.3@outlook.com

Received: 23 May 2021; **Revised:** 27 September 2021; **Accepted:** 02 October 2021

ABSTRACT

Quantitative Ultrasound (QUS) represents an emerging non-invasive imaging approach designed to monitor treatment responses. Research has demonstrated a strong association between QUS backscatter metrics and microscopic structural changes, as variations in ultrasound backscatter parameters significantly reflect increased cell death. Specifically, indicators related to scatterer size and concentration tend to rise with cellular degeneration. Numerous preclinical and clinical investigations have explored the role of QUS in assessing tumor response. Preclinical studies primarily applied QUS to distinguish viable from non-viable cells by assessing cell death dynamics, whereas clinical studies have mainly utilized it for tissue characterization—such as differentiating benign from malignant breast tumors and identifying patients who respond to therapy from those who do not. This review outlines key insights from previous experimental and clinical research, emphasizing the growing clinical potential and therapeutic advantages of QUS. Furthermore, it provides an overview of recent progress in ultrasound-based radiomics for predicting and tracking treatment outcomes, as well as for classifying breast lesions, and addresses the existing limitations, challenges, and future directions of QUS-radiomics in oncology.

Keywords: Chemotherapy, Cell death, Treatment response, Locally advanced breast cancer (LABC), Radiotherapy, Quantitative ultrasound (QUS)

How to Cite This Article: Al-Farsi H, Bader K, Hassan S. Clinical Application of Quantitative Non-Invasive Ultrasound Techniques in Cancer Imaging. Asian J Curr Res Clin Cancer. 2021;1(2):41-55. https://doi.org/10.51847/pXwBXMA1UJ

Introduction

Over time, advancements in technology have significantly contributed to the progress of cancer management. The process of diagnosing cancer remains intricate and involves multiple stages. Diagnostic imaging techniques have been pivotal in enabling early cancer detection. Commonly utilized imaging modalities include computed tomography (CT), magnetic resonance imaging (MRI), positron emission tomography (PET), ultrasound, and X-ray [1, 2]. Among these, Quantitative Ultrasound (QUS) has emerged as a promising approach due to its distinct advantages, including non-invasiveness, affordability, portability, and absence of ionizing radiation [3]. Since QUS imaging does not require surgical intervention or incisions, it is considered a safe and easily accessible technique, extensively studied for both diagnostic and therapeutic applications.

A growing body of preclinical and clinical research has explored the role of QUS in predicting and monitoring cancer progression [4–9]. By performing linear regression analysis on the normalized power spectra of radio frequency (RF) data from ultrasound signals, several key parameters can be derived [10–15]. These linear-fit parameters include the mid-band fit (MBF), spectral intercept at 0 MHz (SI), and spectral slope (SS). The MBF and SI correspond to the degree of backscattered energy, while the SS reflects the relative size of the scattering structures [10–12]. To gain further insights into the characteristics of acoustic scatterers—such as their size and density—measured backscattering data can be fitted to theoretical acoustic scattering models. This fitting yields quantitative metrics including the average scatterer diameter (ASD), effective scatterer diameter (ESD) or size (ESS), and average or effective acoustic concentration (AAC/EAC/ESC). These values can be estimated by applying models like the spherical Gaussian scattering model (SGM) or the fluid-filled-sphere model (FFSM) to

the ultrasonic backscatter coefficient (BSC) [13–15]. Variations in ASD and AAC reflect alterations in scatterer dimensions and density, respectively.

QUS spectral parametric imaging generates visual maps of these quantitative parameters derived from spectral analysis of RF ultrasound data, thereby revealing the inherent scattering properties of tissues. Because tumor tissues exhibit distinct microstructural and scattering characteristics depending on their invasiveness [16] and treatment response [17], QUS spectral maps offer valuable diagnostic [18, 19] and prognostic [20–25] information. These maps are typically produced using a sliding window approach, where a small segment of RF data is analyzed within a moving kernel across the region of interest (ROI). For clinical practice, a 2 mm × 2 mm kernel—approximately equivalent to ten acoustic wavelengths—is often employed. A Hanning gating function is applied axially to smooth the RF data before using the Fast Fourier Transform (FFT) to determine the spectral content. The mean power spectrum for each kernel is then computed by averaging its RF spectra.

To isolate tissue-specific scattering characteristics from the RF signal, the reference phantom technique is used [26, 27]. This approach involves scanning a spatially uniform phantom with known frequency-dependent backscattering and attenuation properties under identical imaging conditions. For each RF block in the tissue sample, a corresponding reference block is obtained from the phantom. Spectral normalization is achieved by dividing the sample spectrum by the reference spectrum, which, combined with attenuation correction and reference BSC values, allows estimation of the tissue's scattering function. The derived frequency-dependent scattering function is then parameterized to obtain diagnostic and prognostic spectral parameters [18–25].

These analyses are repeated throughout the ROI to create comprehensive parametric images of QUS spectral features. From these maps, radiomic features—including first-order statistics, morphology-based, and texture-based attributes—can be extracted. Such radiomic descriptors serve as potential imaging biomarkers for cancer diagnosis and outcome prediction [18–25]. Texture-based radiomic analysis operates on the principle that variations in tissue heterogeneity can be quantitatively represented by the patterns observed in QUS spectral parametric maps **(Figure 1)**.

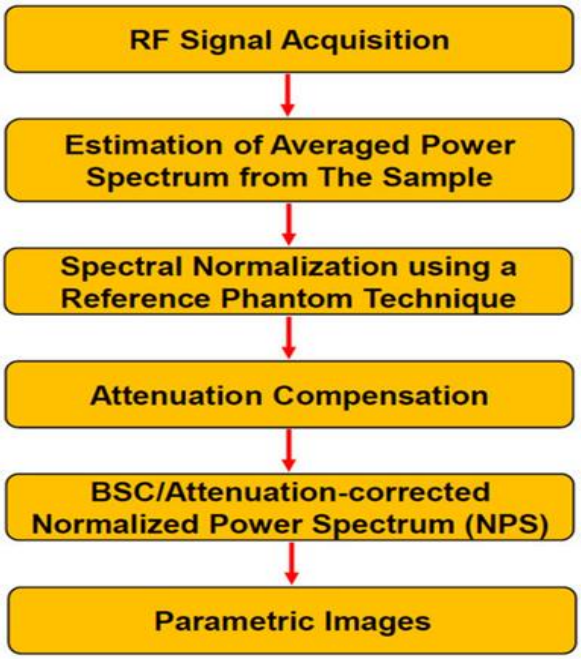

Figure 1. Overview of the QUS spectroscopy workflow. QUS spectroscopy isolates the scattering characteristics embedded in the RF signal, enabling tissue-specific characterization. Through spectral normalization, system-related variations are removed from the RF signal, while attenuation correction compensates for acoustic signal loss as ultrasound waves travel through tissue layers. By parameterizing the attenuation-corrected normalized power spectrum (NPS) or backscatter coefficient (BSC), tumor properties can be quantified to derive diagnostic and prognostic insights. These quantified parameters can subsequently serve as inputs for developing classification models aimed at diagnostic and prognostic applications. Abbreviations: BSC – backscatter coefficient; NPS – normalized power spectrum; QUS – quantitative ultrasound.

Ultrasound imaging of cell death in tumor response

Extensive research has demonstrated a significant relationship between alterations in cell nuclear morphology and variations in ultrasound-derived parameters across both low- and high-frequency modalities. In an in vivo melanoma model, Banihashemi *et al*. reported a time-dependent elevation in the mid-band fit (MBF) and spectral slope (SS) following photodynamic therapy (PDT). After 24 hours, approximately 45% of cells exhibited apoptotic death, coinciding with the peak SS value of 0.435 ± 0.07 dB/MHz. Between 12 and 24 hours, MBF also showed a marked increase, while by 48 hours, around half of the cell nuclei had disappeared due to late-stage apoptosis, resulting in a reduction in ultrasound backscatter signals [28]. This study confirmed a direct association between cellular death progression and QUS parameter variations.

Similar findings were observed in a clinical study by Sadeghi-Naini *et al*., involving patients with locally advanced breast cancer (LABC) undergoing chemotherapy. Their data showed substantial elevations in MBF and spectral intercept (SI) after four weeks of treatment, with responders exhibiting an MBF increase of 9.1 ± 1.2 dBr compared to 1.9 ± 1.1 dBr in non-responders. Likewise, SI values rose to 8.9 ± 1.9 dBr in responders versus 1.6 ± 0.9 dBr in non-responders. Histopathological analysis further supported these findings, showing dense residual tumor tissue in non-responding patients, whereas responders exhibited an absence of such compact masses. These results collectively indicated that favorable treatment response correlates strongly with measurable shifts in QUS parameters [5].

Additional studies have also highlighted that parameters such as average acoustic concentration (AAC) and average scatterer diameter (ASD) are sensitive indicators of cell death. In LABC patients responding to chemotherapy, significant increases in both AAC and ASD were observed at weeks 1, 4, and 8, with the highest elevation noted at week 8, while non-responders showed no such trend [13]. Comparable results were reported in breast cancer xenograft models treated with chemotherapy, where higher AAC values corresponded to greater cell death (approximately 60% at 24 hours), demonstrating a strong correlation between AAC and cell death (R^2_SGM = 0.40) [14].

Overall, these studies collectively underscore the effectiveness of QUS and its derived parameters in assessing treatment-induced cellular changes, monitoring therapeutic outcomes, and distinguishing between patients who respond to treatment and those who do not. The following sections elaborate on key clinical investigations employing QUS for cancer diagnosis, tissue characterization, and prediction or monitoring of treatment response. A concise summary of QUS applications in preclinical and clinical contexts is provided in **Table 1**.

Table 1. Summary of QUS applications and utilization in preclinical and clinical investigations.

QUS Frequency	Application / Implementation	References
50 MHz	Characterization of cell death under in vitro conditions	[29]
40 MHz	Evaluation of treatment response across in vitro, in situ, and in vivo models	[30]
7 MHz	Clinical assessment for tissue characterization	[31]
5.75 MHz	Clinical tissue characterization	[32]
30 MHz and 34 MHz	In vitro analysis of cell death	[33]
4–12 MHz	In vivo tissue characterization	[34]
8 MHz	In vivo tissue differentiation and analysis	[35]
8.5 MHz and 20 MHz	In vivo evaluation of tissue properties	[36]
7.5 MHz	Clinical application for tissue characterization	[37]
40 MHz	In vivo examination of tissue characteristics	[38]
20 MHz	Investigation of structural alterations in cells (in vitro)	[39]
20 MHz	In vivo analysis of tissue composition	[40]
26 MHz	In vivo monitoring of therapeutic response	[28]
20 MHz	In vitro evaluation of therapy response	[41]
20 MHz	In vivo monitoring of treatment response	[42]
1–12 MHz	Phantom-based tissue characterization for clinical use	[43]
25.6 MHz	Clinical evaluation of lymph node characteristics	[44]

25.6 MHz	Clinical assessment of lymph node morphology	[45]
25 MHz	In vivo observation of treatment response	[46]
10 MHz and 15 MHz	Phantom studies for clinical tissue characterization	[47]
7 MHz	Clinical monitoring of treatment outcomes	[5]
25.6 MHz	Detection of lymph node metastases in clinical settings	[48]
~7 MHz and 20 MHz	In vivo monitoring of therapeutic response	[4]
40 MHz	In vivo investigation of tissue properties	[49]
6 MHz	Clinical study of tissue characterization	[50]
25 MHz	In vivo tracking of therapeutic response	[6]
6 MHz	In situ observation of treatment response	[51]
7 MHz	Clinical monitoring of therapy response	[13]
~7 MHz	Combined in vitro and in vivo monitoring of treatment response	[7]
7 MHz and 20 MHz	In vivo analysis of therapeutic effects	[14]
6 MHz	In vivo evaluation of response to therapy	[52]
25 MHz	In vitro study of cell death mechanisms	[53]
25 MHz	In vivo investigation of treatment outcomes	[8]
~6 MHz	Clinical application for tissue differentiation	[54]
29 MHz	Clinical assessment of tissue characteristics	[55]
6.5 MHz and 6.9 MHz	Clinical prediction of treatment response	[21]
6.3 MHz and 7 MHz	Clinical monitoring of therapeutic progression	[56]
8 MHz	Clinical observation of treatment effects	[57]
7 MHz	Clinical prediction of therapy response	[58]
6.5 MHz	Prediction of tumor recurrence in clinical settings	[59]
6.5 MHz	Clinical prediction of treatment response	[19]
7 MHz	Clinical evaluation of tumor recurrence prediction	[25]
7 MHz	Clinical prediction of tumor recurrence	[60]

Clinical applications of classification models developed from QUS spectral parametric images using machine learning approaches

Tumor characterization

Beyond its established role in monitoring therapeutic response and evaluating treatment effectiveness, Quantitative Ultrasound (QUS) has also been extensively investigated for its ability to differentiate between benign and malignant tumors [54, 61, 62]. One of the earliest studies in this area, conducted by Sadeghi-Naini *et al*., employed QUS spectral and texture-based analysis to characterize breast lesions in 78 patients. The study quantified intra-lesional heterogeneity by combining textural parameters with mean-value features derived from various QUS parametric maps, providing insights into tissue microstructural organization [54]. Subsequently, Osapoetra *et al*. expanded upon this work by including a larger cohort and analyzing both texture and texture-derivative features within peri-tumoral breast tissue regions [61]. These studies primarily relied on texture analysis based on the Gray Level Co-occurrence Matrix (GLCM) to distinguish between benign and malignant breast lesions. Later, Osapoetra *et al*. further enhanced their approach by integrating multiple texture analysis methods—namely GLCM, Gray Level Run Length Matrix (GLRLM), and Gray Level Size Zone Matrix (GLSZM)—applied to QUS spectral parametric images from both the tumor core and margin to improve lesion characterization [62]. In another study, Sadeghi-Naini *et al*. evaluated a range of texture features to discriminate benign from malignant breast lesions. Given that QUS texture parameters reflect the underlying size, density, and spatial distribution of acoustic scatterers, they can be leveraged to quantify intra-tumoral heterogeneity, offering valuable insights into tissue microarchitecture. The study extracted texture features such as contrast (CON), correlation (COR), homogeneity (HOM), and energy (ENE) from QUS parametric maps including mid-band fit (MBF), spectral slope

(SS), spectral intercept (SI), spacing among scatterers (SAS), effective acoustic concentration (EAC), and effective scatterer diameter (ESD). These metrics were then utilized as imaging biomarkers for lesion classification. Statistically significant distinctions ($p < 0.05$) were observed between benign and malignant groups in several parameters, notably MBF (CON, COR, HOM), SS (CON, COR, HOM), SI (CON, COR, HOM), SAS (ENE), ESD (CON, COR), and EAC (HOM, ENE) [54].

Further expanding this diagnostic approach, Osapoetra *et al*. applied QUS spectral parametric imaging and texture analysis for breast lesion characterization in a larger clinical dataset [61, 62]. They developed classification models by combining radiomic features extracted from QUS parametric maps with conventional machine learning algorithms to distinguish between malignant and benign lesions. The authors proposed that texture-derivative features possess strong discriminative potential for multi-feature classification modeling. Their study analyzed data from 204 patients (99 with benign and 105 with malignant breast lesions). Representative B-mode, ASD, AAC, MBF, SS, and SI parametric maps for both lesion types are shown in **Figures 2 and 3**, while **Figure 4** presents scatter and box plots illustrating key discriminating features. Among the extracted features, texture-derivative metrics provided the clearest separation between lesion types. The final model achieved optimal classification performance, with 90% sensitivity, 92% specificity, 91% overall accuracy, and an area under the curve (AUC) of 0.93 when using features derived from both the tumor core and margin [61].

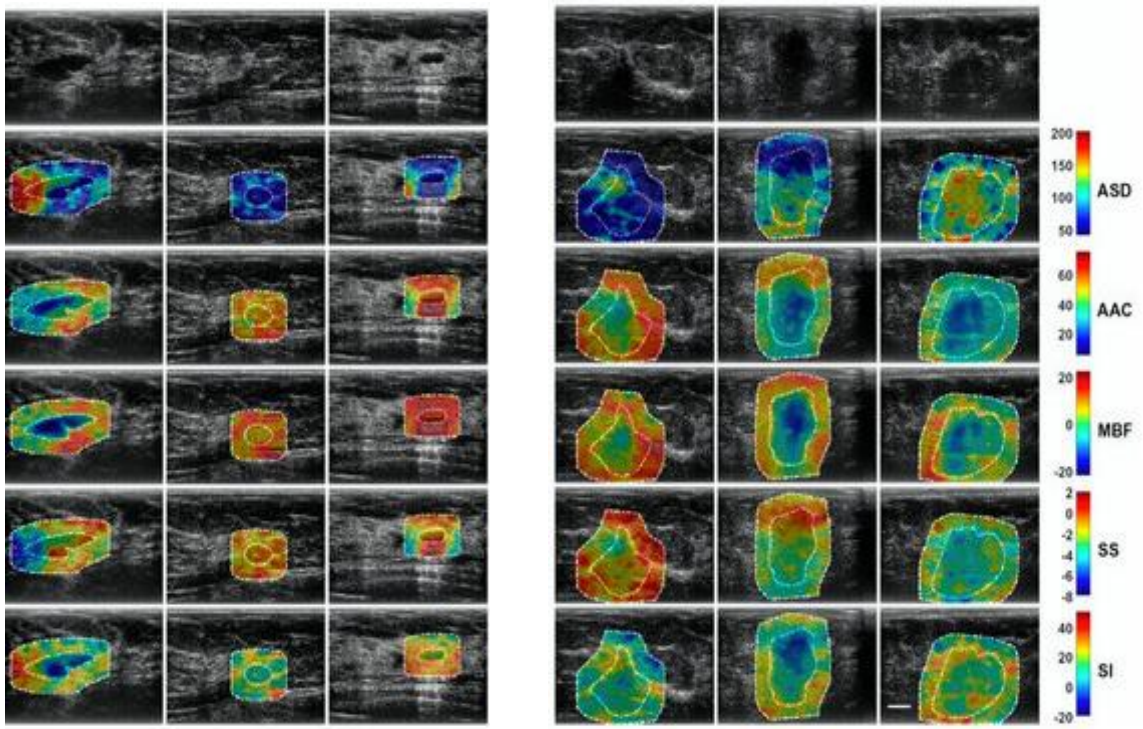

a) b)

Figure 2. Illustration of representative QUS spectral parametric maps from both benign and malignant breast lesions. (a) displays benign lesions (left columns), while (b) shows malignant counterparts (right columns). The color gradients indicate the quantitative parameter ranges, including ASD up to 160 μm, AAC up to 70 dB/cm³, MBF up to 44 dB, SS up to 10 dB/MHz, and SI up to 70 dB. A 1 cm scale bar is provided for reference. Abbreviations: ASD – average scatterer diameter; AAC – average acoustic concentration; MBF – mid-band fit; SS – spectral slope; SI – 0-MHz intercept. Adapted with permission from **(Figure 1)** [61].

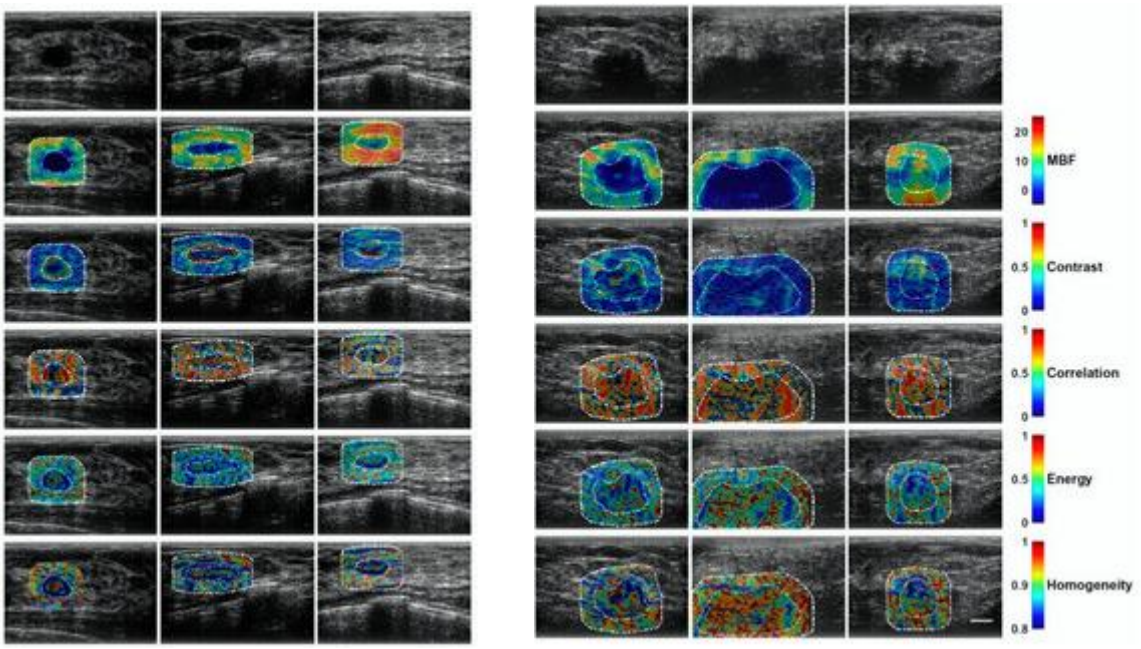

a) b)

Figure 3. Example texture maps demonstrating localized quantification of image texture in breast lesions. (a) shows benign lesions (left columns), while (b) illustrates malignant lesions (right columns). The scale bar represents 1 cm. Abbreviation: MBF – mid-band fit. Reprinted with permission from: **(Figure 2)** [61].

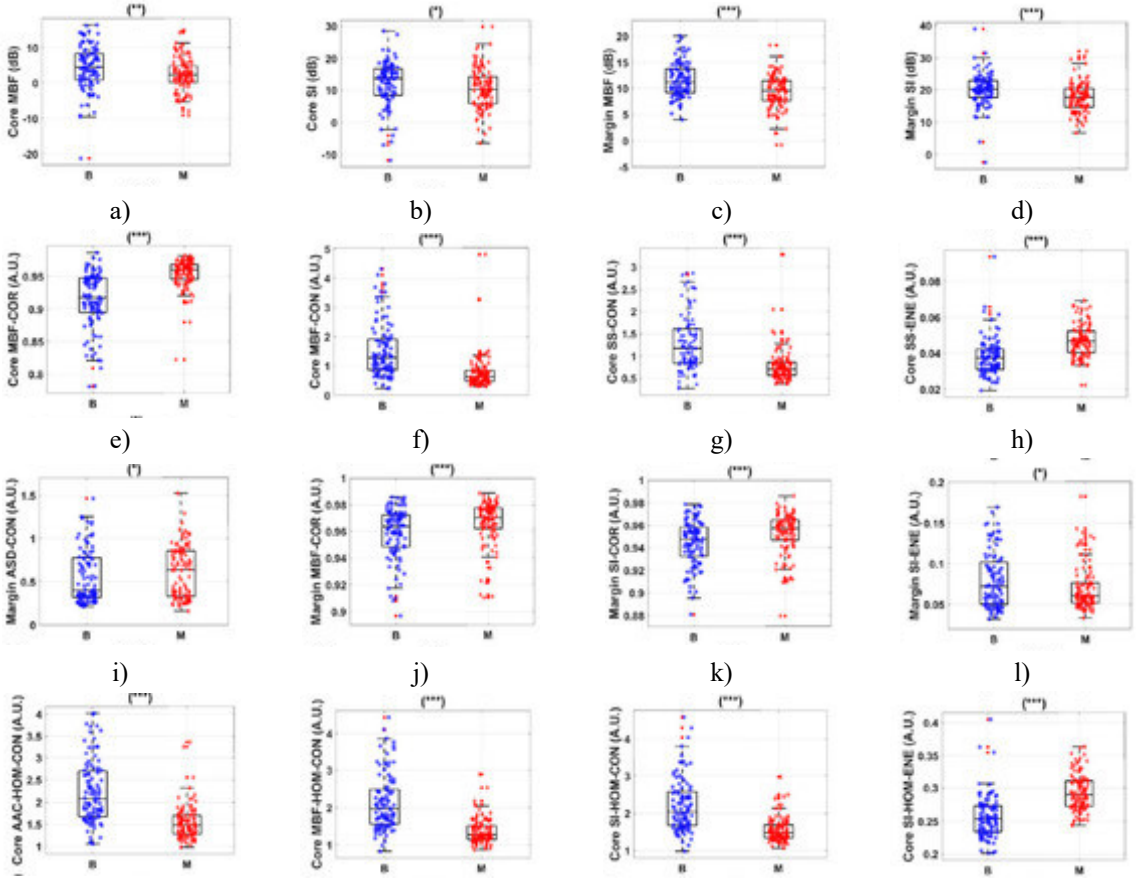

a) b) c) d)

e) f) g) h)

i) j) k) l)

m) n) o) p)

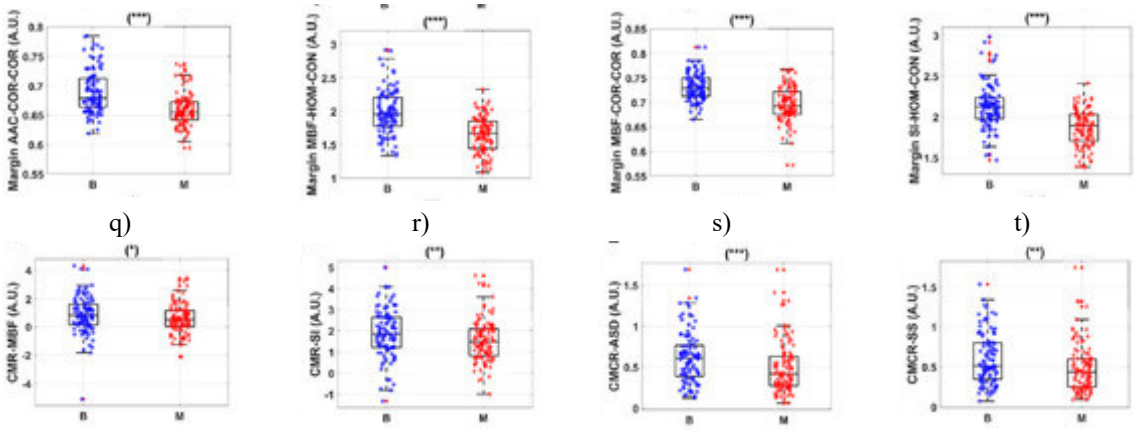

q) r) s) t)

u) v) w) x)

Figure 4. Boxplots and scatter plots illustrating representative radiomics features with statistically significant differences, denoted as (* $p < 0.05$), (** $p < 0.01$), and (*** $p < 0.001$). B indicates benign breast lesions, M indicates malignant breast lesions, ASD is average scatterer diameter, AAC is average acoustic concentration, MBF is mid-band fit, SS is spectral slope, SI is 0-MHz intercept, CON is contrast, COR is correlation, ENE is energy, and HOM is homogeneity. Reprinted with permission from: **(Figure 3)** [61].

In a separate investigation, various methods for quantifying image textures were explored to characterize breast lesions. Classification models were built using radiomics features derived from GLCM, GLRLM, and GLSZM analyses of QUS spectral parametric images. Depending on tumor characteristics, margin attributes, and the classification algorithm employed, the models achieved accuracies ranging from 73% to 91% across a cohort of 193 patients, which included 92 benign and 101 malignant lesions [62].

QUS spectroscopy has also been applied to other cancer types. For instance, Rohrbach *et al*. utilized QUS for non-invasive assessment of prostate cancer via a novel high-frequency transrectal ultrasound system (ExactVu micro-ultrasound, Exact Imaging, Markham, ON, Canada). They combined ASD, AAC, envelope statistics, and prostate-specific antigen (PSA) data into a multivariate model, reaching a maximum AUC of 0.81 using a linear discriminant classifier [55]. Similarly, Goundan *et al*. conducted a study on thyroid nodule (TN) characterization, analyzing 225 TNs (24 malignant, 201 benign) from 208 patients [63]. Their classification model incorporated QUS spectral parameters (ASD, AAC, MBF, SI) along with an envelope statistics feature in the Nakagami shape parameter, achieving an ROC AUC of 0.857 ± 0.033, comparable to ACR TI-RADS and ATA risk-stratification systems. Additionally, their results indicated that combining QUS features—alone or with ACR TI-RADS—could reduce unnecessary fine-needle biopsies [63].

LABC QUS treatment response prediction

QUS spectral parametric imaging and texture analyses have been explored for predicting cancer treatment response. The premise is that QUS spectral parameters are sensitive enough to detect microscopic tumor changes, which can serve as imaging biomarkers for constructing classification models. Clinically, such models can inform early interventions, guiding treatment modifications. For example, in neoadjuvant chemotherapy (NAC) for LABC, predicting non-responders early enables clinicians to adjust therapy, optimizing tumor reduction prior to surgery.

Recent studies have developed QUS-based prediction models for LABC treatment response [20–23, 25]. These investigations addressed multiple aspects: using higher-order GLCM-based textural features for model development [21, 24]; evaluating variability of radiomics features across different ultrasound systems [20]; validating models with multi-institutional data [18, 21]; extracting features from intra-tumoral regions via unsupervised segmentation [22]; and implementing deep learning approaches [23].

Dasgupta *et al*. examined models utilizing higher-order texture-derivative features in a cohort of 100 LABC patients undergoing NAC (83 responders, 17 non-responders) [58]. Radiomics features included first-order mean values, GLCM-based texture, and GLCM-based texture-derivatives. Sequential feature selection identified the optimal feature set, yielding models with 87% sensitivity, 81% specificity, 82% accuracy, and 0.86 AUC [58].

Sannachi *et al*. addressed potential variations in radiomics features across different ultrasound systems, analyzing 24 LABC patients using GE-LOGIQ E9 (GE Healthcare) and Ultrasonix-RP (Ultrasonix Medical Corp.) machines

[20]. They applied a previously developed classification model and found minimal system-specific differences, with tissue heterogeneity identified as the main source of feature variation, and model performance remained consistent across systems **(Table 2, Figures 5 and 6)** [20].

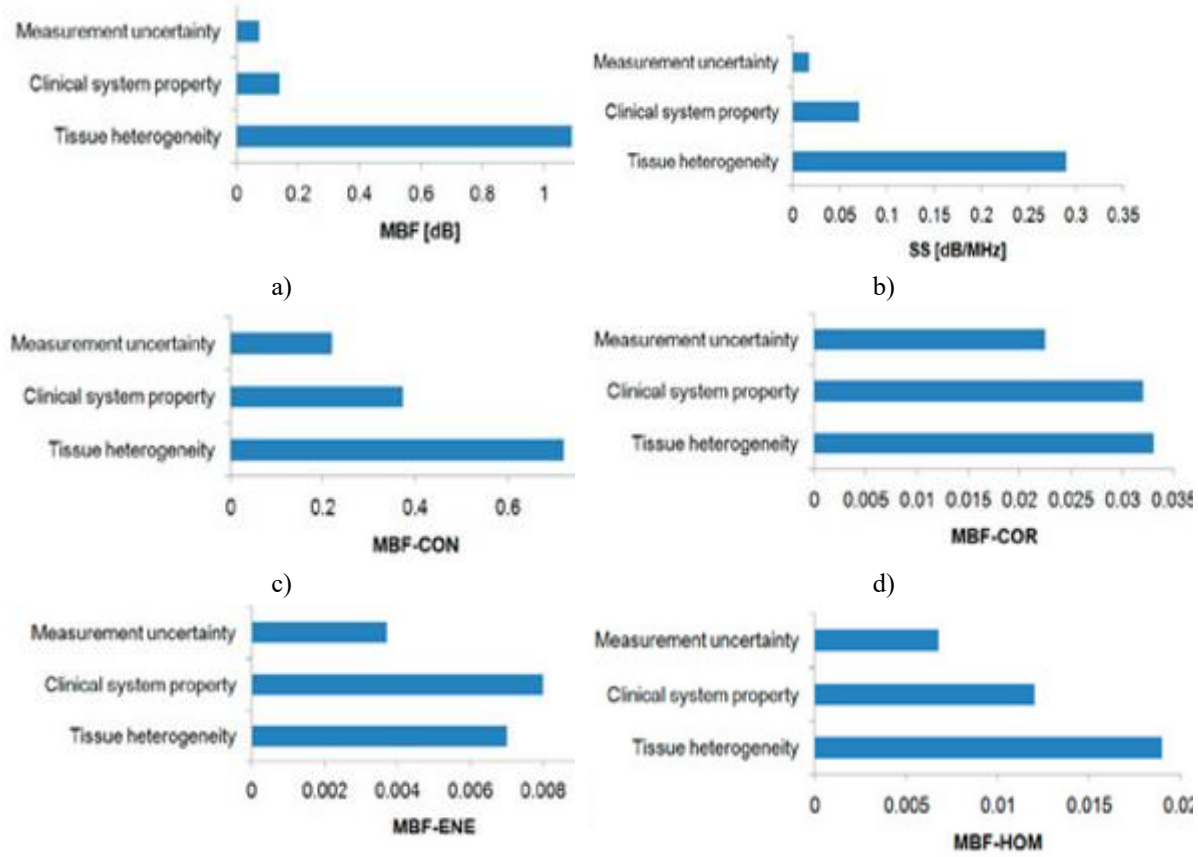

Figure 5. Root mean square deviations in QUS parameters—MBF and SS—as well as MBF-texture features (MBF-CON, MBF-COR, MBF-ENE, MBF-HOM) arising from measurement uncertainty, differences between ultrasound systems, and tissue heterogeneity. The findings indicate that intrinsic tissue heterogeneity is the primary factor driving variability in radiomics features derived from QUS spectral parametric images, whereas measurement uncertainty and system-related differences contribute comparatively less. MBF: mid-band fit, SS: spectral slope, CON: contrast, COR: correlation, ENE: energy, HOM: homogeneity. Reprinted with permission from: **(Figure 3)** [20].

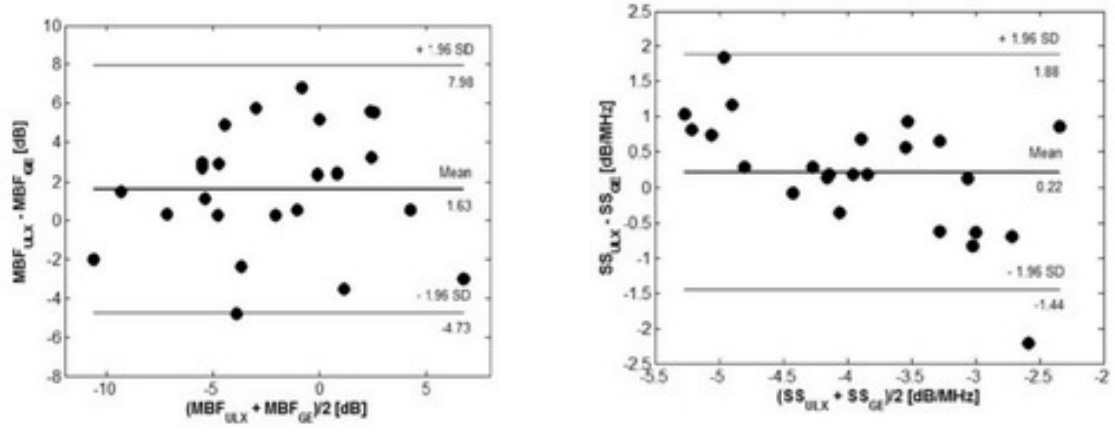

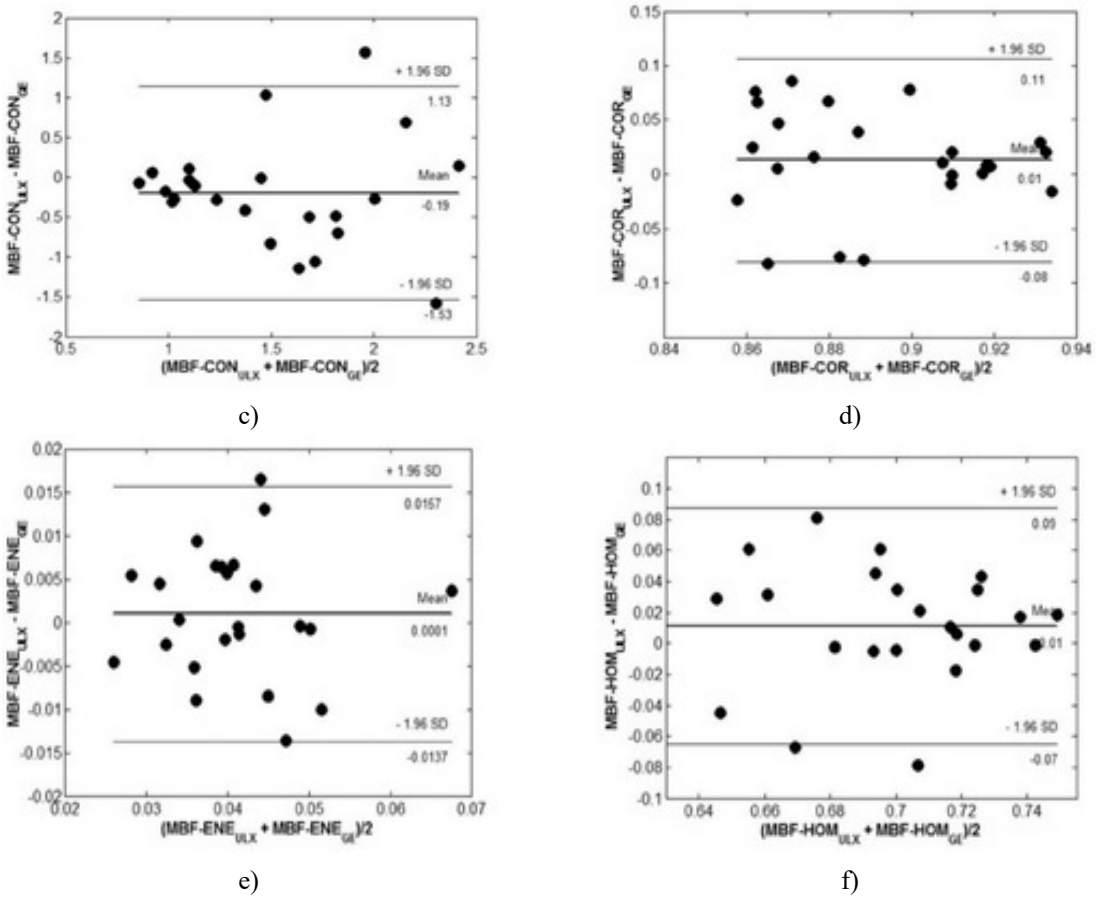

Figure 6. Bland-Altman analysis was performed to compare radiomics features extracted from two ultrasound platforms: the Ultrasonix-RP (Ultrasonix Medical Corp., Richmond, BC, Canada) and the GE-LOGIQ E9 (General Electric Healthcare, Milwaukee, WI, USA). The agreement limits were calculated as the mean difference ± standard deviation. MBF represents mid-band fit, SS is spectral slope, CON is contrast, COR is correlation, ENE is energy, HOM is homogeneity, ULX refers to Ultrasonix RP L14-5/60, and GE corresponds to GE-LOGIQ 9 L-D. Reprinted with permission from: **(Figure 6)** [20].

Table 2. Classification results for identifying non-responders versus responders at weeks 1, 4, and 8 after chemotherapy initiation using data from the two ultrasound systems. Statistically significant discrepancies between the systems are marked with an asterisk (*) ($p < 0.05$). The predictive model applied for monitoring treatment response was adapted from prior work. Abbreviations: US, ultrasound; ULX, ULX L14-5/60; GE, GE-LOGIQ E9. Adapted with permission from [20].

Scan Time	US System	Sensitivity [%]	Specificity [%]	Accuracy [%]	McNemar p *
Week 1	ULX	60.0	50.0	58.8	0.752
	GE	60.0	50.0	58.8	
Week 4	ULX	78.9	66.7	77.3	0.545
	GE	64.3	66.7	69.1	
Week 8	ULX	71.4	100.0	73.3	0.683
	GE	71.4	100.0	73.3	

DiCenzo *et al*. evaluated the effectiveness of a classification model for predicting therapy response in LABC patients using multi-institutional data. Their study included 82 patients undergoing NAC, comprising 48 responders and 34 non-responders. Pre-treatment radiomics features, including first-order statistical mean values and GLCM-based texture measures, were used to develop the models, achieving a maximum accuracy of 87% in distinguishing non-responders from responders [21]. Building on this, Osapoetra *et al*. investigated a similar multi-institutional cohort of 74 patients (42 responders, 32 non-responders) and incorporated additional higher-

order GLCM texture features in their models. Their analysis demonstrated the discriminative power of higher-order textures for breast lesion characterization, resulting in a classification performance of 88% sensitivity, 78% specificity, 84% accuracy, and an AUC of 0.86 [18].

Traditionally, radiomics-based treatment response models estimate mean values or average texture features across the entire QUS spectral parametric image. In contrast, Taleghamar *et al*. proposed a method that leverages spatial information within intra-tumoral parametric maps. Their technique first segments discrete tumor regions using an unsupervised approach based on a hidden Markov random field (HMRF) with expectation maximization (EM). Radiomics features were then extracted from specific intra-tumoral regions rather than the entire tumor. In a cohort of 181 LABC patients (138 responders, 43 non-responders), pre-treatment QUS features included first-order statistical mean values and signal-to-noise ratio (SNR). Using the Adaptive Boosting (AdaBoost) algorithm, their model achieved 85.4% accuracy and an AUC of 0.89 on an independent test set [22].

Deep learning methods, which learn hierarchical feature representations directly from data rather than relying on engineered features, have established state-of-the-art performance in computer vision, natural language processing, and other domains [39, 64]. Motivated by these advances, Taleghamar *et al*. implemented deep learning approaches to improve the prediction of treatment response from QUS spectral parametric images [23]. Unlike prior deep learning studies using B-mode images, their network inputs were parametric QUS images [22]. They employed convolutional neural networks (CNNs) with modified ResNet-101 and residual attention network (RAN-56) architectures as base layers, topped with a densely connected classifier. Trained from scratch using augmented QUS images, the model applied to 181 LABC patients (138 responders, 43 non-responders) achieved a peak performance of 88% accuracy and 0.86 AUC on an independent test set [23].

Head and neck QUS treatment response prediction

QUS radiomics has also been applied to predict therapy response in head and neck squamous cell carcinoma (HNSCC). A cohort of 59 patients—22 early responders (ER), 29 late responders (LR), and 8 with progressive disease (PD)—undergoing radical radiotherapy (with or without concurrent chemotherapy) was analyzed. Classification models were designed to separate non-responders (NR) from responders (R) and further distinguish late responders from those with persistent or progressive disease [19]. **Table 3** presents metrics for classifying ER versus partial or non-responders, while **Table 4** summarizes the performance for LR versus persistent or progressive disease. **Figure 7** illustrates a representative decision boundary and the distribution of the two groups in a three-dimensional feature space using the top three selected features [19].

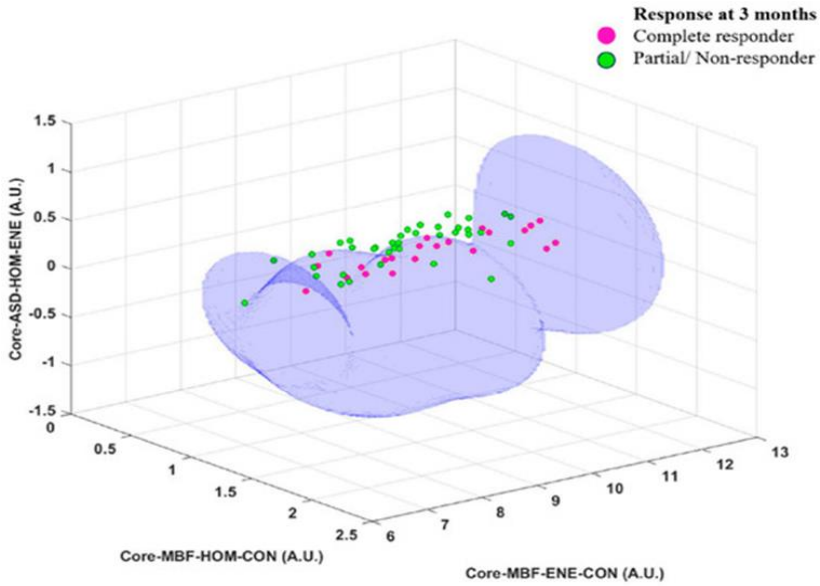

Figure 7. Example of a nonlinear decision boundary generated by a support vector machine (SVM) with a radial basis function (RBF) kernel, used to distinguish complete responders from partial or non-responders. The model utilized the optimal set of three radiomics features, selected via forward sequential feature selection with cross-validation. Abbreviations: SVM, support vector machine; RBF, radial basis function; MBF, mid-band fit; CON, contrast; ENE, energy; HOM, homogeneity. Reprinted with permission from: **(Figure 3)** [19].

Table 3. Three-month response outcomes comparing complete responders (early responders, n = 22) with partial/non-responders (n = 37), highlighting the performance of classification models in identifying complete responders. Among the methods tested, the SVM-RBF model achieved the highest performance for this classification task. Abbreviations: FLD, Fisher's linear discriminant; KNN, k-nearest neighbors; SVM-RBF, support vector machine with radial basis function; MBF, mid-band fit; SI, 0-MHz intercept; SS, spectral slope; ASD, average scatterer diameter; AAC, average acoustic concentration; COR, correlation; CON, contrast; HOM, homogeneity; ENE, energy. Adapted with permission from [19].

Classifier	Sensitivity	Specificity	Accuracy	AUC	Selected Features
FLD	73	81	78	0.75	MBF-HOM-CON, MBF, SI-CON-ENE
KNN	73	84	80	0.80	SS-COR-COR, MBF-ENE-HOM
SVM-RBF	86	95	92	0.91	MBF-HOM-CON, MBF-ENE-CON, ASD-HOM-ENE

Table 4. Final treatment response comparing late responders (n = 29) with patients exhibiting persistent or progressive disease (n = 8). The performance of classification models—including Fisher's linear discriminant (FLD), k-nearest neighbors (KNN), and support vector machine with radial basis function kernel (SVM-RBF)—is summarized. Radiomics features considered in the analysis included MBF (mid-band fit), SI (0-MHz intercept), SS (spectral slope), ASD (average scatterer diameter), AAC (average acoustic concentration), CON (contrast), COR (correlation), ENE (energy), and HOM (homogeneity). Adapted with permission from [19].

Classifier	Sensitivity	Specificity	Accuracy	AUC	Selected Features
FLD	86	100	89	0.92	AAC-ENE-HOM, AAC-HOM-CON
KNN	93	88	92	0.90	AAC-HOM, ASD-ENE-HOM
SVM-RBF	97	88	95	0.97	SS, SS-HOM-CON

Tran *et al*. [57] evaluated classification models to predict treatment response following radical radiotherapy in head and neck cancer patients. Their cohort included 36 individuals, comprising 14 complete responders (CR) and 22 partial responders (PR). Models were constructed using the most informative features from a set of radiomics attributes, which included first-order statistical mean values and GLCM-based texture metrics extracted from QUS spectral parametric images obtained at 24 hours, 1 week, and 4 weeks post-treatment. The models achieved classification accuracies of 80%, 86%, and 85% at the three respective time points [57].

Recurrence prediction

Head and neck cancer

Radiomics of QUS spectral parametric images has also been applied for recurrence prediction in 51 patients with head and neck squamous cell carcinoma (HNSCC) treated with radiotherapy, with or without concurrent chemotherapy (17 recurrences, 34 non-recurrences) [24, 59]. Dasgupta *et al*. used traditional machine learning models trained on pre-treatment radiomics features, including first-order mean statistics and GLCM-based textures. Their best-performing model, using a k-nearest neighbors (KNN) classifier, achieved 76% sensitivity, 71% specificity, 75% accuracy, and an AUC of 0.74 [24]. In a similar cohort, Fatima *et al*. incorporated delta-radiomics, calculating feature changes between pre-treatment and week 1 and week 4 post-treatment QUS images. Their classification models reported accuracies of 80% and 82% at weeks 1 and 4, respectively [59].

Locally advanced breast cancer (LABC)

For LABC, Dasgupta *et al*. developed a pre-treatment QUS radiomics-based model to predict recurrence in 83 patients (28 recurrences, 55 non-recurrences) undergoing NAC. Features included first-order statistics, GLCM-based textures, and higher-order GLCM textures. Using an SVM classifier, the model achieved 71% sensitivity, 87% specificity, 82% accuracy, and 0.76 AUC. Five-year recurrence-free survival was 83% for predicted non-recurrences versus 54% for predicted recurrences ($p = 0.003$), with corresponding overall survival rates of 85% versus 74% ($p = 0.083$) [25]. Bhardwaj *et al*. analyzed the same cohort using baseline and week 4 radiomics features, achieving 87% sensitivity, 75% specificity, 81% accuracy, and 0.83 AUC [60].

Conclusion

QUS and its spectral parameters provide a rapid, non-invasive approach to monitor treatment response, differentiate responders from non-responders, and characterize tumors as benign or malignant. Unlike traditional methods that rely on tumor size measurement over days or weeks, QUS can detect tissue morphological changes within hours. Early identification of tumor heterogeneity and treatment response using QUS may allow timely adjustments in therapy.

Radiomics applied to QUS spectral parametric imaging has demonstrated broad utility for tumor characterization, treatment response monitoring, and recurrence prediction. However, careful implementation is necessary, as these approaches rely on training with labeled data and generalization to unseen datasets. Current efforts focus on refining model-building and evaluation strategies to avoid pitfalls such as information leakage from training to validation or test sets. Overall, QUS-derived radiomics features hold promise for developing robust computer-aided diagnostic (CAD) systems capable of guiding clinical cancer therapy.

Limitations and future directions

Several limitations exist for QUS. As a handheld modality, reproducibility is less certain compared to automated techniques like mammography or MRI. Many studies are retrospective and single-center, raising concerns about model stability and generalizability across different systems. Although normalization and attenuation correction help reduce system-specific variations in RF signals, standardized measurements across institutions, trials, and ultrasound platforms are needed to ensure reproducibility.

Interlaboratory studies, such as that by Anderson *et al*. [43], demonstrate the feasibility of consistent ultrasound backscatter coefficient (BSC) measurements. Using phantom materials with known scatterer distributions, multiple institutions assessed BSC across transducers with varying frequencies, bandwidths, apertures, and focal lengths. Excellent agreement was observed between laboratories, confirming accurate estimation of BSC-derived parameters, including linear fit and scattering metrics. Expanding such inter-institutional studies would provide larger, diverse datasets to further enhance the reliability and accuracy of QUS radiomics-based predictive models.

Acknowledgments: None

Conflict of Interest: None

Financial Support: None

Ethics Statement: None

References

1. Fass L. Imaging and cancer: a review. Mol Oncol. 2008;2(2):115–52.
2. Frangioni JV. New Technologies for Human Cancer Imaging. J Clin Oncol. 2008;26(24):4012–21.
3. Oelze ML, Mamou J. Review of Quantitative Ultrasound: Envelope Statistics and Backscatter Coefficient Imaging and Contributions to Diagnostic Ultrasound. IEEE Trans Ultrason Ferroelectr Freq Control. 2016;63(2):336–51.
4. Sadeghi-Naini A, Papanicolau N, Falou O, Tadayyon H, Lee J, Zubovits J, et al. Low-frequency quantitative ultrasound imaging of cell death in vivo. Med Phys. 2013;40(8):082901.
5. Sadeghi-Naini A, Papanicolau N, Falou O, Zubovits J, Dent R, Verma S, et al. Quantitative Ultrasound Evaluation of Tumor Cell Death Response in Locally Advanced Breast Cancer Patients Receiving Chemotherapy. Clin Cancer Res. 2013;19(8):2163–74.
6. Kim HC, Al-Mahrouki A, Gorjizadeh A, Sadeghi-Naini A, Karshafian R, Czarnota GJ. Quantitative Ultrasound Characterization of Tumor Cell Death: Ultrasound-Stimulated Microbubbles for Radiation Enhancement. PLoS One. 2014;9(7):e102343.
7. Sadeghi-Naini A, Zhou S, Gangeh MJ, Jahedmotlagh Z, Falou O, Ranieri S, et al. Quantitative evaluation of cell death response in vitro and in vivo using conventional-frequency ultrasound. Oncoscience. 2015;2(8):716–26.
8. Tran WT, Sannachi L, Papanicolau N, Tadayyon H, Al Mahrouki A, El Kaffas A, et al. Quantitative ultrasound imaging of therapy response in bladder cancer in vivo. Oncoscience. 2016;3(2):122–33.

9. Sharma D, Osapoetra LO, Faltyn M, Do NN A, Giles A, Stanisz M, et al. Quantitative ultrasound characterization of therapy response in prostate cancer in vivo. Am J Transl Res. 2021;13(9):4437–49.
10. Sadeghi-Naini A, Falou O, Tadayyon H, Al-Mahrouki A, Tran W, Papanicolau N, et al. Conventional Frequency Ultrasonic Biomarkers of Cancer Treatment Response In Vivo. Transl Oncol. 2013;6(3):234–43.
11. Lizzi FL, Ostromogilsky M, Feleppa EJ, Rorke MC, Yaremko MM. Relationship of Ultrasonic Spectral Parameters to Features of Tissue Microstructure. IEEE Trans Ultrason Ferroelectr Freq Control. 1987;34(3):319–29.
12. Lizzi FL, Astor M, Feleppa EJ, Shao M, Kalisz A. Statistical framework for ultrasonic spectral parameter imaging. Ultrasound Med Biol. 1997;23(9):1371–82.
13. Sannachi L, Tadayyon H, Sadeghi-Naini A, Tran W, Gandhi S, Wright F, et al. Non-invasive evaluation of breast cancer response to chemotherapy using quantitative ultrasonic backscatter parameters. Med Image Anal. 2015;20(2):224–36.
14. Tadayyon H, Sannachi L, Sadeghi-Naini A, Al-Mahrouki A, Tran WT, Kolios MC, et al. Quantification of Ultrasonic Scattering Properties of In Vivo Tumor Cell Death in Mouse Models of Breast Cancer. Transl Oncol. 2015;8(6):463–73.
15. Ghoshal G, Luchies AC, Blue JP, Oelze ML. Temperature dependent ultrasonic characterization of biological media. J Acoust Soc Am. 2011;130(4):2203–11.
16. Frank GA, Danilova NV, Andreeva YY, Nefedova NA. WHO classification of tumors of the breast, 2012. Arkh Patol. 2013;75(1):53–63.
17. Ogston KN, Miller ID, Payne S, Hutcheon AW, Sarkar TK, Smith I, et al. A new histological grading system to assess response of breast cancers to primary chemotherapy: prognostic significance and survival. Breast. 2003;12(5):320–7.
18. Osapoetra LO, Sannachi L, Quiaoit K, Dasgupta A, DiCenzo D, Fatima K, et al. A priori prediction of response in multicentre locally advanced breast cancer (LABC) patients using quantitative ultrasound and derivative texture methods. Oncotarget. 2021;12(1):81–94.
19. Osapoetra LO, Dasgupta A, DiCenzo D, Fatima K, Quiaoit K, Saifuddin M, et al. Assessment of clinical radiosensitivity in patients with head-neck squamous cell carcinoma from pre-treatment quantitative ultrasound radiomics. Sci Rep. 2021;11(1):6117.
20. Sannachi L, Gangeh M, Sadeghi-Naini A-S, Bhargava P, Jain A, Tran WT, et al. Quantitative Ultrasound Monitoring of Breast Tumour Response to Neoadjuvant Chemotherapy: Comparison of Results Among Clinical Scanners. Ultrasound Med Biol. 2020;46(5):1142–57.
21. DiCenzo D, Quiaoit K, Fatima K, Bhardwaj D, Sannachi L, Gangeh M, et al. Quantitative ultrasound radiomics in predicting response to neoadjuvant chemotherapy in patients with locally advanced breast cancer: Results from multi-institutional study. Cancer Med. 2020;9(16):5798–806.
22. Taleghamar H, Moghadas-Dastjerdi H, Czarnota GJ, Sadeghi-Naini A. Characterizing intra-tumor regions on quantitative ultrasound parametric images to predict breast cancer response to chemotherapy at pre-treatment. Sci Rep. 2021;11(1):14865.
23. Taleghamar H, Jalalifar SA, Czarnota GJ, Sadeghi-Naini A. Deep learning of quantitative ultrasound multi-parametric images at pre-treatment to predict breast cancer response to chemotherapy. Sci Rep. 2022;12(1):2244.
24. Dasgupta A, Fatima K, DiCenzo D, Bhardwaj D, Quiaoit K, Saifuddin M, et al. Quantitative ultrasound radiomics in predicting recurrence for patients with node-positive head-neck squamous cell carcinoma treated with radical radiotherapy. Cancer Med. 2021;10(6):2579–89.
25. Dasgupta A, Bhardwaj D, DiCenzo D, Fatima K, Osapoetra LO, Quiaoit K, et al. Radiomics in predicting recurrence for patients with locally advanced breast cancer using quantitative ultrasound. Oncotarget. 2021;12(3):2437–48.
26. Yao LX, Zagzebski JA, Madsen EL. Backscatter Coefficient Measurements Using a Reference Phantom to Extract Depth-Dependent Instrumentation Factors. Ultrason Imaging. 1990;12(1):58–70.
27. Labyed Y, Bigelow TA, McFarlin BL. Estimate of the attenuation coefficient using a clinical array transducer for the detection of cervical ripening in human pregnancy. Ultrasonics. 2011;51(1):34–9.
28. Banihashemi B, Vlad R, Debeljevic B, Giles A, Kolios MC, Czarnota GJ, et al. Ultrasound Imaging of Apoptosis in Tumor Response: Novel Preclinical Monitoring of Photodynamic Therapy Effects. Cancer Res. 2008;68(20):8590–6.

29. Czarnota GJ, Kolios MC, Vaziri H, Benchimol S, Ottensmeyer FP, Sherar MD, et al. Ultrasonic biomicroscopy of viable, dead and apoptotic cells. Ultrasound Med Biol. 1997;23(6):961–5.
30. Czarnota GJ, Kolios MC, Abraham J, Portnoy M, Ottensmeyer FP, Hunt JW, et al. Ultrasound imaging of apoptosis: High-resolution non-invasive monitoring of programmed cell death in vitro, in situ and in vivo. Br J Cancer. 1999;81(3):520–7.
31. Feleppa EJ, Ennis RD, Schiff PB, Wuu CS, Kalisz A, Ketterling J, et al. Spectrum-analysis and neural networks for imaging to detect and treat prostate cancer. Ultrason Imaging. 2001;23(2):135–46.
32. Feleppa EJ, Ennis RD, Schiff PB, Wuu CS, Kalisz A, Ketterling J, et al. Ultrasonic spectrum-analysis and neural-network classification as a basis for ultrasonic imaging to target brachytherapy of prostate cancer. Brachytherapy. 2002;1(1):48–53.
33. Kolios MC, Czarnota GJ, Lee M, Hunt JW, Sherar MD. Ultrasonic spectral parameter characterization of apoptosis. Ultrasound Med Biol. 2002;28(5):589–97.
34. Oelze ML, Zachary JF, O'Brien WD Jr. Characterization of tissue microstructure using ultrasonic backscatter: theory and technique for optimization using a Gaussian form factor. J Acoust Soc Am. 2002;112(3):1202–11.
35. Oelze ML, Zachary JF, O'Brien WD Jr. Parametric imaging of rat mammary tumors in vivo for the purposes of tissue characterization. J Ultrasound Med. 2002;21(11):1201–10.
36. Oelze ML, O'Brien WD Jr, Blue JP, Zachary JF. Differentiation and Characterization of Rat Mammary Fibroadenomas and 4T1 Mouse Carcinomas Using Quantitative Ultrasound Imaging. IEEE Trans Med Imaging. 2004;23(6):764–71.
37. Feleppa EJ, Porter CR, Ketterling J, Lee P, Dasgupta S, Urban S, et al. Recent Developments in Tissue-Type Imaging (TTI) for Planning and Monitoring Treatment of Prostate Cancer. Ultrason Imaging. 2004;26(3):163–72.
38. Vlad RM, Czarnota GJ, Giles A, Sherar MD, Hunt JW, Kolios MC. High-frequency ultrasound for monitoring changes in liver tissue during preservation. Phys Med Biol. 2005;50(1):197–213.
39. Tunis AS, Czarnota GJ, Giles A, Sherar MD, Hunt JW, Kolios MC. Monitoring structural changes in cells with high-frequency ultrasound signal statistics. Ultrasound Med Biol. 2005;31(8):1041–9.
40. Oelze ML, Zachary JF. Examination of cancer in mouse models using high-frequency quantitative ultrasound. Ultrasound Med Biol. 2006;32(11):1639–48.
41. Vlad RM, Alajez NM, Giles A, Kolios MC, Czarnota GJ. Quantitative Ultrasound Characterization of Cancer Radiotherapy Effects In Vitro. Int J Radiat Oncol Biol Phys. 2008;72(5):1236–43.
42. Vlad RM, Brand S, Giles A, Kolios MC, Czarnota GJ. Quantitative Ultrasound Characterization of Responses to Radiotherapy in Cancer Mouse Models. Clin Cancer Res. 2009;15(7):2067–75.
43. Anderson JJ, Herd M-T, King MR, Haak A, Hafez ZT, Song J, et al, Madsen EL, Zagzebski JA, O'Brien WD Jr, et al. Interlaboratory Comparison of Backscatter Coefficient Estimates for Tissue-Mimicking Phantoms. Ultrason Imaging. 2010;32(1):48–64.
44. Mamou J, Coron A, Hata M, Machi J, Yanagihara E, Laugier P, et al. Three-Dimensional High-Frequency Characterization of Cancerous Lymph Nodes. Ultrasound Med Biol. 2010;36(3):361–75.
45. Mamou J, Coron A, Oelze ML, Saegusa-Beecroft E, Hata M, Lee P, et al. Three-Dimensional High-Frequency Backscatter and Envelope Quantification of Cancerous Human Lymph Nodes. Ultrasound Med Biol. 2011;37(2):345–57.
46. Lee J, Karshafian R, Papanicolau N, Giles A, Kolios MC, Czarnota GJ. Quantitative Ultrasound for the Monitoring of Novel Microbubble and Ultrasound Radiosensitization. Ultrasound Med Biol. 2012;38(7):1212–21.
47. Nam K, Zagzebski JA, Hall TJ. Quantitative Assessment of In Vivo Breast Masses Using Ultrasound Attenuation and Backscatter. Ultrason Imaging. 2013;35(2):146–61.
48. Saegusa-Beecroft E, Machi J, Mamou J, Hata M, Coron A, Yanagihara ET, et al. Three-dimensional quantitative ultrasound for detecting lymph node metastases. J Surg Res. 2013;183(1):258–69.
49. Lavarello RJ, Ridgway WR, Sarwate SS, Oelze ML. Characterization of Thyroid Cancer in Mouse Models Using High-Frequency Quantitative Ultrasound Techniques. Ultrasound Med Biol. 2013;39(12):2333–41.
50. Tadayyon H, Sadeghi-Naini A, Wirtzfeld L, Wright FC, Czarnota GJ. Quantitative ultrasound characterization of locally advanced breast cancer by estimation of its scatterer properties. Med Phys. 2014;41(1):012903.

51. Ghoshal G, Kemmerer JP, Karunakaran C, Abuhabsah R, Miller RJ, Sarwate S, et al. Quantitative ultrasound imaging for monitoring in situ high-intensity focused ultrasound exposure. Ultrason Imaging. 2014;36(3):239–55.
52. Ghoshal G, Kemmerer JP, Karunakaran C, Miller RJ, Oelze ML. Quantitative Ultrasound for Monitoring High-Intensity Focused Ultrasound Treatment In Vivo. IEEE Trans Ultrason Ferroelectr Freq Control. 2016;63(8):1234–42.
53. Pasternak MM, Wirtzfeld LA, Kolios MC, Czarnota GJ. High-Frequency Ultrasound Analysis of Post-Mitotic Arrest Cell Death. Oncoscience. 2016;3(3):109–21.
54. Sadeghi-Naini A, Suraweera H, Tran WT, Hadizad F, Bruni G, Rastegar RF, et al. Breast-Lesion Characterization using Textural Features of Quantitative Ultrasound Parametric Maps. Sci Rep. 2017;7(1):13638.
55. Rohrbach D, Wodlinger B, Wen J, Mamou J, Feleppa E. High-Frequency Quantitative Ultrasound for Imaging Prostate Cancer Using a Novel Micro-Ultrasound Scanner. Ultrasound Med Biol. 2018;44(6):1341–54.
56. Quiaoit K, DiCenzo D, Fatima K, Bhardwaj D, Sannachi L, Gangeh M, et al. Quantitative ultrasound radiomics for therapy response monitoring in patients with locally advanced breast cancer: Multi-institutional study results. PLoS ONE. 2020;15(6):e0236182.
57. Tran WT, Suraweera H, Quiaoit K, DiCenzo D, Fatima K, Jang D, et al. Quantitative ultrasound delta-radiomics during radiotherapy for monitoring treatment responses in head and neck malignancies. Future Sci OA. 2020;6(7):1–15.
58. Dasgupta A, Brade S, Snnachi L, Quiaoit K, Fatima K, DiCenzo D, et al. Quantitative ultrasound radiomics using texture derivatives in prediction of treatment response to neo-adjuvant chemotherapy for locally advanced breast cancer. Oncotarget. 2020;11(4):3782–92.
59. Fatima K, Dasgupta A, DiCenzo D, Kolios C, Quiaoit K, Saifuddin M, et al. Ultrasound delta-radiomics during radiotherapy to predict recurrence in patients with head and neck squamous cell carcinoma. Clin Transl Radiat Oncol. 2021;28:62–70.
60. Bhardwaj D, Dasgupta A, DiCenzo D, Brade S, Fatima K, Quiaoit K, et al. Early Changes in Quantitative Ultrasound Imaging Parameters during Neoadjuvant Chemotherapy to Predict Recurrence in Patients with Locally Advanced Breast Cancer. Cancers. 2022;14(5):1247.
61. Osapoetra LO, Sannachi L, DiCenzo D, Quiaoit K, Fatima K, Czarnota GJ. Breast lesion characterization using Quantitative Ultrasound (QUS) and derivative texture methods. Transl Oncol. 2020;13(10):100827.
62. Osapoetra LO, Chan W, Tran W, Kolios MC, Czarnota GJ. Comparison of methods for texture analysis of QUS parametric images in the characterization of breast lesions. PLoS ONE. 2020;15(4):e0244965.
63. Goundan PN, Mamou J, Rohrbach D, Smith J, Patel H, Wallace KD, et al. A Preliminary Study of Quantitative Ultrasound for Cancer-Risk Assessment of Thyroid Nodules. Front Endocrinol (Lausanne). 2021;12:627698.
64. Najafabadi MM, Villanustre F, Khoshgoftaar TM, Seliya N, Wald R, Muharemagic E. Deep learning applications and challenges in big data analytics. J Big Data. 2015;2(1):1.